18TH WORLD CONFERENCE ON EARTHQUAKE ENGINEERING
WCEE2024
MILAN

MILAN, ITALY
30TH JUNE - 5TH JULY 2024

www.wcee2024.it

SEISMIC VULNERABILITY ASSESSMENT OF PRECAST POST-TENSIONED SEGMENTAL PIERS

S.Kocakaplan Sezgin[1], E. Ahmadi[2] & M.M. Kashani[3]

[1] Bursa Technical University, Bursa, Turkey, sedef.kocakaplan@btu.edu.tr

[2] Birmingham City University, Birmingham, United Kingdom

[3] University of Southampton, Southampton, United Kingdom

Abstract: *Precast post-tensioned segmental (PPS) bridge piers mitigate global and local damages of bridge structures through natural hinges. The application of PPS piers has increased recently in Accelerated Bridge Construction (ABC). Therefore, to increase their use in high-seismicity regions, this paper examines seismic vulnerability assessment of post-tensioned segmental bridge piers with Shape Memory Alloy (SMA) bars through a Finite Element (FE) framework. First, to investigate the energy dissipation capacity of the PPS piers with SMA, an extensive parametric study performed on the key design parameters including, (i) number of segments or aspect ratio, (ii) length, area, and post-tensioning of the SMA bars, and (iii) area and post-tensioning of the tendon. The results are also compared with the piers without SMA bars. Furthermore, an equivalent reinforced concrete (RC) pier to one of the PPS piers is also analysed. Incremental dynamic analysis (IDA) is performed, and fragility curves are generated to evaluate seismic performance of the PPS piers with and without SMA bars using a suite of 44 far-fault ground motions. The IDA results show that, slenderizing the PPS piers tends to change failure criterion from the yielding of the post-tensioning tendon to strength loss of the pier. For squat piers, the yielding of the tendon governs the failure of the pier while for very slender PPS piers, the strength of PPS piers drops due to second-order effects at small drift values prior to the yielding of the post-tensioning tendon. Furthermore, the equivalent RC pier reaches slight and medium damage states in lower intensity measures compared to the PPS piers. Finally, IDA results of PPS piers with SMA bars show that their median IDA curves for drift responses are lower than the ones without SMA bars.*

1 Introduction

The research on the performance of precast post-tensioned segmental (PPS) piers is increasing to design a bridge structure with less vulnerability and longer lifespan. Unlike the cast-in-place (CIP) piers, which are integrally constructed and connected to their base, the rocking motion of the PPS piers prevents development of large concrete cracks. Further, the post-tensioned tendon causes the PPS pier to return to its origin after lateral seismic ground motions. Many experimental and numerical studies were carried out to understand static and dynamic behaviour of the PPS piers.

Many experimental and numerical studies examined performance of the PPS piers primarily subject to cyclic and dynamic loadings (Billington and Yoon 2004, Hassanli et al. 2010, Wang and Wang 2018, Wang et al. 2018, Ou et al. 2008, Chou and Chen 2006, Motaref et al. 1994, Zhang and Hao 2019, Dawood et al. 2012, Ahmadi and Kashani 2020). Furthermore, to increase the use of PPS piers in highly seismic regions, low energy dissipation capacity of the piers should be addressed. A method to increase the dissipation capacity of the structures is the use of super-elastic Shape Memory Alloy (SMA) bars. It is well known that SMA bars can

dissipate energy of the structure through their nonlinear deformations and return to their initial state after loading events (Song et al. 2006, DesRoches and Delemont 2002).

This study focuses on seismic performance assessment of the PPS piers using Incremental Dynamic Analysis (IDA) tool. The piers are subject to an ensemble of actual ground motion records (far-field and pulse-like ground motions). Furthermore, IDA analysis is also performed for the piers with SMA bars that are subjected to far-field ground motions and results are compared with the piers without SMA bars. The SMA bars are used at the edge of the segments to increase damping capability of the pier and improve self-centering capacity of the entire pier.

2 The Proposed PPS Piers

Performance of three PPS piers with various aspect ratios are studied in this research. As illustrated in Figure 1, the PPS piers are composed of a number of segments, n, of width B, where the total height of the piers is denoted by H. The axial load from the bridge deck is described as a fraction of the axial capacity of the concrete section, $N/(f_cA_g)$, where N is the axial load, f_c and A_g are the concrete compressive strength and the total cross section area of each pier, respectively. The segments are stabilized by a stainless-steel tendon, which is attached to the base and to the top of the pier. The tendon creates a self-centering property and returns the piers to their initial state after any lateral loading.

Table 1 illustrates the piers and their properties used in this research. The piers are 1, 2, and 4 m high, and are composed of 2, 4, and 8 square segments. The post-tensioning tendon ratios, $\rho = A_t/A_g$ (tendon-to-segment area ratio), of 0.005, 0.01, and 0.02 are selected respectively for the 2, 4, and 8-segment piers such that all piers have the same stiffness for the tendon, E_tA_t/H. E_t and A_t are the elastic modulus and area of the tendon respectively. Constant axial load ratio, $N/(f_cA_g)$ = 0.2, and initial post-tensioning-to-yield stress ratio, σ^0_t/σ_y = 0.4, are selected for the tendon of the piers.

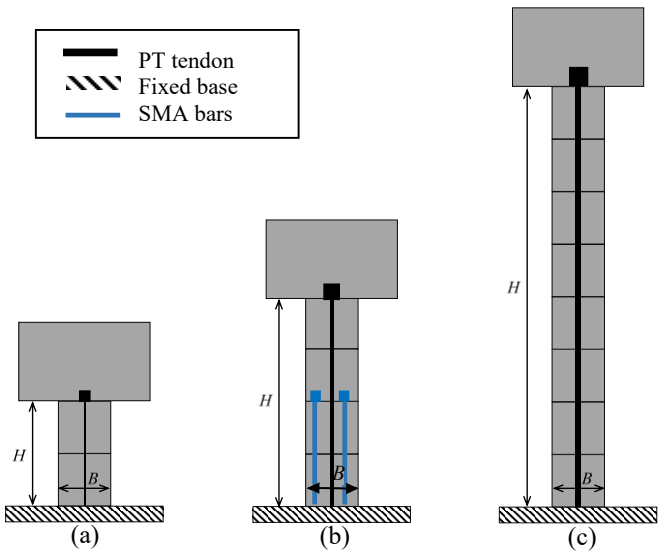

Figure 1. Schematic view of the PPS piers used in this study: (a) 2 segments, C2 (b) 4 segments, C4, and (c) 8 segments, C8.

The individual segments of the pier are tightened together using an unbonded post-tensioning stainless steel tendon (see Figure1a and Figure 1b). The tendon provides a self-centering mechanism in the pier when subjected to lateral loading or any unbalance moment. Unbonded post-tensioned super-elastic NiTi SMA bars are used at the bottom segments to increase energy dissipation capacity of the pier (see Figure 1a and Figure 1b). The axial load from the top deck is defined as a ratio of the axial load to the axial capacity of the concrete section, $N/(f_cA_g)$, where N is the axial load, f_c and A_g are the concrete compressive strength and the total cross section area of the segment, respectively. The concrete strength, f_c, is taken 35 MPa in this study.

Table 1. Details of PPs piers used in this study.

Column Label	*n* (number of segments)	*H* (m)	*B* (m)	*ρ*	$N/(f_cA_g)$	σ^0_t/σ_y
C2	2	1	0.5	0.005	0.2	0.4
C4	4	2	0.5	0.01	0.2	0.4
C8	8	4	0.5	0.02	0.2	0.4

The FE modelling of the pier can be found in (Ahmadi and Kashani 2020). The two-dimensional (2D) FE model of the pier is developed in the program OpenSees (McKenna 2011). Elastic Beam-Column elements are used for the modelling of the segments. The segments are connected through nodes with three degrees-of-freedom: one horizontal translations, one vertical translation, and one rotation. The sliding between segments and accordingly frictional damping is discarded in the modelling. This is because the diameter of the hole within the segment is slightly larger than the tendon diameter, and hence, the segments are not allowed to slide on top of each other. The post-tensioned tendon is modelled with a Truss Element and an Elastic Perfectly Plastic material. An initial strain was implemented into the material model to account for post-tensioning force of the tendon. Yield stress, σ_y, and elastic modulus of the tendon are 1860 MPa and 200 GPa respectively. For the tendon, post-tensioning is defined as post-tensioning-to-yield stress, σ_t/σ_y. Corotational geometric transformation is used for Beam-Column and Truss elements to account for their geometric nonlinearities. Inertial effects of the bridge deck are considered by applying lumped horizontal and vertical masses to the top node of the pier. These masses are equivalent to the axial force acting on the pier.

For piers with SMA bars, piers with same height as pier C4 are used during this study (See Figure 1b.). The post-tensioned SMA bars are modelled using Truss Elements. Figure 2 shows the idealized flag-shape constitutive model used for the SMA (Tazarv and Saiid Saiidi 2015). As seen in Figure 2, SMA is a self-centered material, and recovers its original shape after unloading. The tension and compression behaviors are identical. Table 2 summarizes the parameters used for the SMA material model in this work (Li et al. 2017). Post-tensioning ratio of the SMA bars, α_{SMA}, is defined as $\sigma^0_{SMA}/\sigma_{SAM}$, where σ^0_{SMA} is the initial post-tensioning stress in SMA bars, and σ_{SAM} is the start stress at austenite-to-martensite transformation phase, σ_{SAM} (see Table 2 and Figure 2). The SMA material model with initial post-tensioning stress was coded and implemented in OpenSees by the authors.

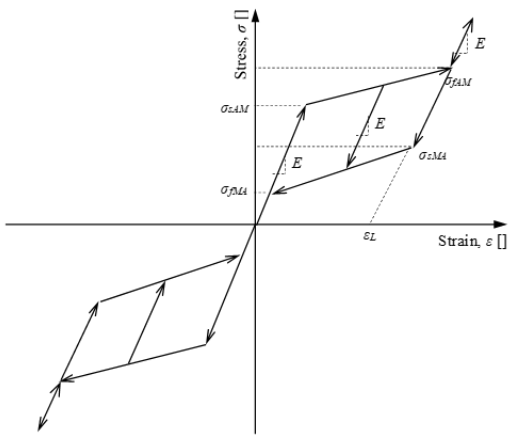

Figure 2. Idealized constitutive model of SMA material implemented by the authors in OpenSees.

Table 2. SMA parameters used in this study (Li et al. 2017).

Parameters	***Describtion***	***Value***
E	Initial modulus of elasticity	68.2 GPa
ε_L	Volumetric transformation strain	0.06
σ_{SAM}	Start stress at austenite-to-martensite transformation phase	480 MPa
σ_{fAM}	Finish stress at austenite-to-martensite transformation phase	540 MPa
σ_{SMA}	Start stress at martensite-to-austenite transformation phase	260 MPa
σ_{fMA}	Finish stress at martensite-to-austenite transformation phase	120 MPa

3 Analysis and Results

In this section, the IDA analyses are performed on the pier models in Section 2 using the ground motions in Section 3.1. The intensity measure (IM) selected for the IDA analysis in this study is the 5% damped spectral acceleration response of the ground motions at the pier's first mode period, S_a *(*T_1*, 5%).* T1 is the first natural vibration period of the pier at very low-amplitude dynamic excitations where the joints are still close, and no rocking motion has initiated. This period is determined using eigenvalue analysis of the piers. The first natural periods of the C2, C4, and C8 piers are 0.09s, 0.26s, and 0.75s respectively. The higher the column becomes the longer its natural period is. Prior to the IDA analysis of each pier, the ground motions are first scaled to 1 at the natural period of each pier using their 5% damped spectra. The IM is then changed from 0.05g to 1g with the increment of 0.05g. Small IM value of 0.005g very close to 0 is also considered to ensure elastic behaviour of the piers before their rocking initiation.

Furthermore, a parametric study is performed to investigate nonlinear static and dynamic behaviour of the SMA-equipped PPS piers. A nonlinear static analysis is performed for a different range of parameters and the piers having the highest energy dissipation capacity are chosen for the dynamic analysis (See Table 3).

Table 3. Representative piers for dynamic analysis.

Piers	***αt***	ρ_t	α_{sma}	ρ_{sma}
A0	0.6	0.020	0.0	0.0
A1	0.6	0.020	0.6	0.025
A2	0.6	0.020	0.3	0.025
B0	0.4	0.020	0.0	0.00
B1	0.4	0.020	0.3	0.025
B2	0.4	0.020	0.6	0.025
C0	0.2	0.020	0.0	0.00
C1	0.2	0.020	0.6	0.025
C2	0.2	0.020	0.3	0.025

3.1 Selected Ground Motions

A set of 44 far-fault ground motion records are used for the seismic assessment of the piers. The ground motions are those recommended in FEMA P659 (Applied Technology Council 2009) and are composed of 22 component pairs of horizontal ground motions from sites located within a distance greater than 10 km from fault rupture.

Further, IDA analysis is also performed for the piers without SMA bars that are subjected to pulse-like ground motions. The ground motion set used herein consists of 40 pulse-like ground motions. These ground motions contain strong velocity pulses of varying periods in their strike-normal components, as determined using the methods described by Baker (Baker 2007) (See Appendix and (Ahmadi et al. 2022)). One benefit of the technique used by Baker (Baker 2007) for the identification of the pulses is to extract the pulse portion from the original ground motion (OGM), which is here named as pulse ground motion (PGM). The subtraction of the PGM from the OGM gives the residual portion of the ground motion, which is here called non-pulse ground motion (NPGM).

3.2 IDA Curves

For the following figures, the top drift is defined as the displacement of the tip of the pier normalised by the total height of the pier, Δ/H. The base shear is normalised by the total weight of the pier including the segments and the top mass, W.

3.2.1 Far Field Ground Motions

Figure 3 compares median IDA curves of all three piers for various responses. For small IM values, as the pier becomes slenderer, the top drift becomes larger (see Figure 3a). The reason lies in the fact that slender piers require smaller minimum ground excitation to start their rocking motion. However, at higher IM values, the squat pier gives higher top drift as all the piers have initiated their rocking motion. The median IDA curves of the base rotation exhibit the same trend as the top drift (Figure 3b). The only difference is the IM value at which the effect of the aspect ratio becomes reversed. This IM value is larger for the top drift.

3.2.2 Pulse-Like Ground Motions

Herein, due to page limits, only the results of a short period ground motion are presented. Figures 4 and 5 show IDA curves of the piers C4, and C8 for top drift, base rotation, normalised base shear, and normalised base moment subject to record no. 9 with extracted pulse period of 0.952s. This record has the lowest pulse period among all 40 records. As seen in Figure 4, the effect of the PGM on the pier C4 is very small, which is well justified by the fact that the first natural frequency of the pier falls far below the pulse period of the PGM. Thus, C4 is not excited by the PGM. The effects of the PGM and NPGM become different for the pier C8. As seen in Figure 5, the effects of the PGM are far greater than the NPGM. In this case, the effect of the OGM is well presented by a single pulse motion, PGM. This is because the period of the pier C8, 0.75s, is close enough to the pulse period, 0.95s, so that the first mode of the pier is excited by the PGM.

3.2.3 Piers with SMA bars

PPS piers with SMA bars are only subjected to 44 far-fault ground motions. Figure 6 shows the median IDA curves for piers C0, C1 and C2 in Table 3. According to figure, median curves of top drift and normalised based rotation for the piers with no SMA bars C0 resulted in higher responses compared to the piers with SMA bars. However, the responses for normalised based shear and normalised based moment resulted of the piers without SMA bars follows a lower response due to additional stiffness of the SMA bars.

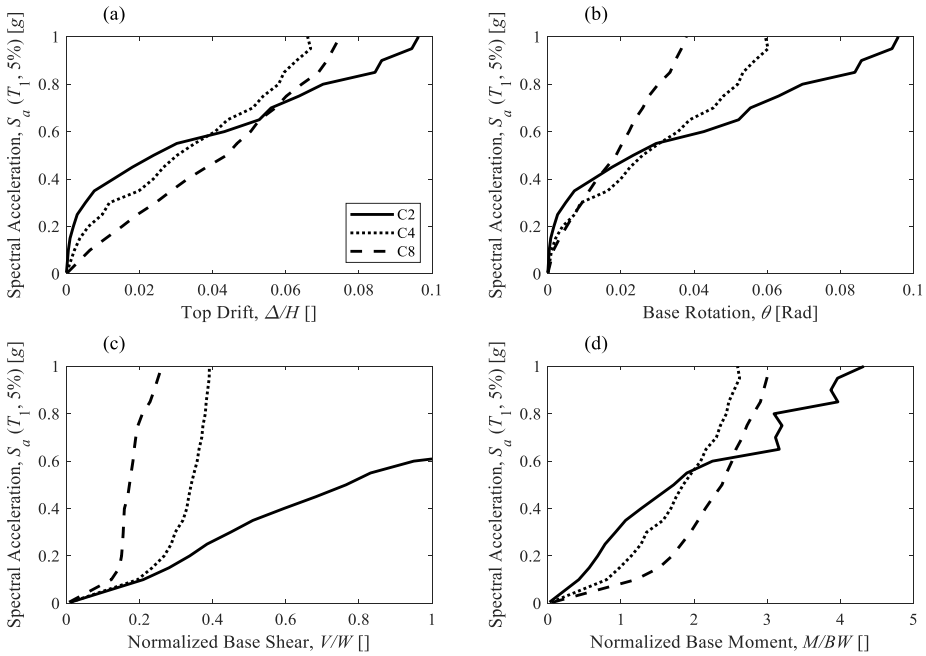

Figure 3. Median IDA curves of all far field ground motions for the piers: (a) top drift, (b) base rotation, (c) normalised base shear, and (d) normalised base moment.

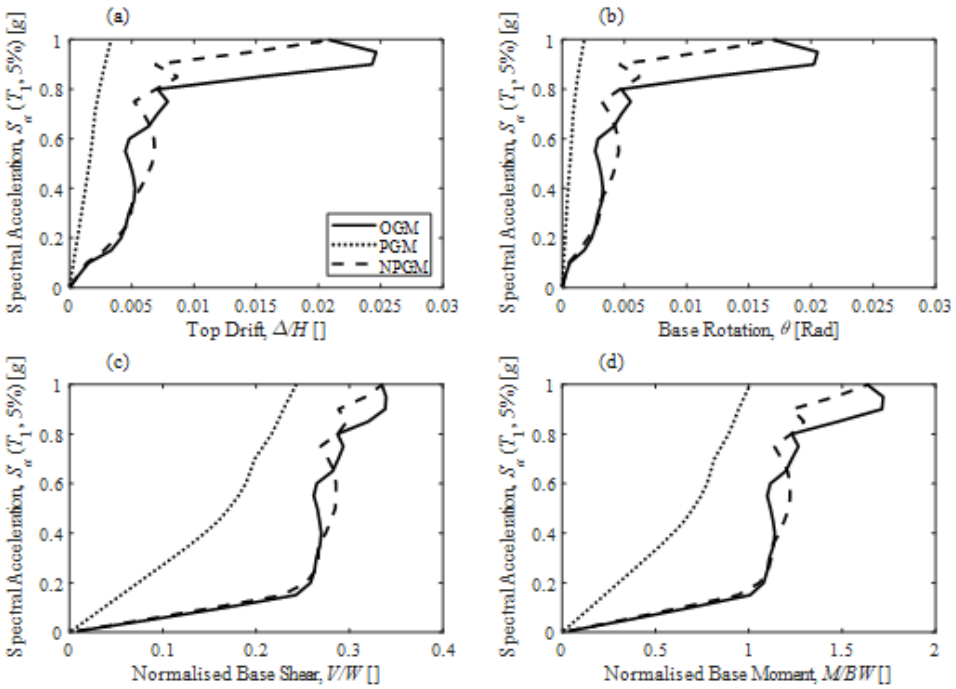

Figure 4. IDA curves of record no. 9 for the pier C4: (a) top drift, (b) base rotation, (c) normalised base shear, and (d) normalised base moment.

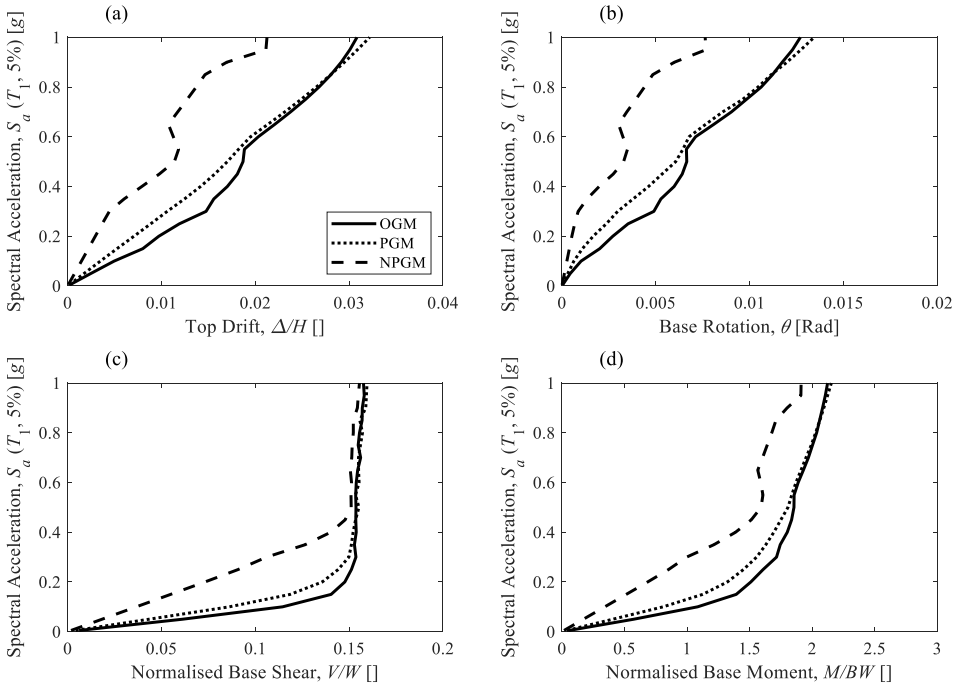

Figure 5. IDA curves of record no. 9 for the pier C8: (a) top drift, (b) base rotation, (c) normalised base shear, and (d) normalised base moment.

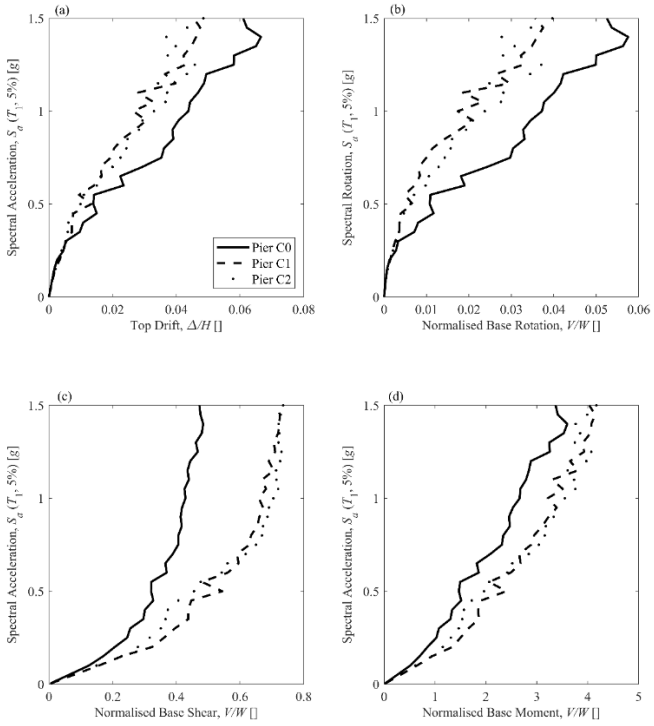

Figure 6. Median IDA curves of all ground motions for the piers C0, C1, and C2: (a) top drift, (b) base rotation, (c) normalised base shear, and (d) normalised base moment.

4 Conclusions

In this study, seismic performance of precast post-tensioned segmental piers is investigated using IDA analyses. An experimentally validated FE model is used to simulate dynamic behaviour of three piers with different aspect ratios subject to an extensive ensemble of 44 far-fault ground motions and 40 pulse-like ground motions. It was found from the median IDA curves of the piers that slenderising the pier increases the top drift, base rotation, and base moment. According to results of IDA analysis for pulse-like ground motions, the IDA curves of the piers demonstrate that the pulse-to-pier period ratio plays a vital role in significance of the pulse ground motion. If this ratio is in the vicinity of 1, meaning the pulse period is close to the natural period of the pier, the effect of the pulse ground motion is pronounced, and the effect of the non-pulse ground motion is negligible. Conversely, if the pulse-to-pier period ratio is far from 1, the non-pulse ground motion is dominant, and the effect of the pulse ground motion is insignificant. Finally, the IDA results show that SMA bars can significantly reduce the drift responses of the piers. Furthermore, besides providing energy dissipation capacity, SMA bars also increase the stiffness of the system.

Acknowledgements

The authors acknowledge the support received by the UK Engineering and Physical Sciences Research Council (EPSRC) for a Prosperous Nation [grant number EP/R039178/1]: SPINE: Resilience-Based Design of Biologically Inspired Columns for Next-Generation Accelerated Bridge Construction]

5 Appendix

Table A1. The near-fault ground motion ensemble.

Record number	Earthquake Name	Year	Station Name	Magnitude	Pulse Period (s)
1	Imperial Valley-06	1979	EC County Center FF	6.53	4.51
2	Imperial Valley-06	1979	EC Meloland Overpass FF	6.53	3.35
3	Imperial Valley-06	1979	El Centro Array #4	6.53	4.61
4	Imperial Valley-06	1979	El Centro Array #5	6.53	4.05
5	Imperial Valley-06	1979	El Centro Array #6	6.53	3.84
6	Imperial Valley-06	1979	El Centro Array #7	6.53	4.23
7	Imperial Valley-06	1979	El Centro Array #8	6.53	5.39
8	Imperial Valley-06	1979	El Centro Differential Array	6.53	5.86
9	Morgan Hill	1984	Coyote Lake Dam (SW Abut)	6.19	0.95
10	Loma Prieta	1989	Gilroy - Gavilan Coll.	6.93	1.79
11	Loma Prieta	1989	LGPC	6.93	4.39
12	Landers	1992	Lucerne	7.28	5.10
13	Landers	1992	Yermo Fire Station	7.28	7.50
14	Northridge-01	1994	Jensen Filter Plant	6.69	3.53
15	Northridge-01	1994	Jensen Filter Plant Generator	6.69	3.53
16	Northridge-01	1994	Newhall - Fire Sta	6.69	1.04
17	Northridge-01	1994	Newhall - W Pico Canyon Rd.	6.69	2.41
18	Northridge-01	1994	Rinaldi Receiving Sta	6.69	1.23
19	Northridge-01	1994	Sylmar - Converter Sta	6.69	3.48
20	Northridge-01	1994	Sylmar - Converter Sta East	6.69	3.53
21	Northridge-01	1994	Sylmar - Olive View Med FF	6.69	3.11
22	Kobe, Japan	1995	KJMA	6.90	0.95
23	Kobe, Japan	1995	Takarazuka	6.90	1.43
24	Kocaeli, Turkey	1999	Gebze	7.51	5.79
25	Chi-Chi, Taiwan	1999	CHY028	7.62	2.24
26	Chi-Chi, Taiwan	1999	CHY101	7.62	4.59
27	Chi-Chi, Taiwan	1999	TCU049	7.62	11.65
28	Chi-Chi, Taiwan	1999	TCU052	7.62	8.36
29	Chi-Chi, Taiwan	1999	TCU053	7.62	12.84
30	Chi-Chi, Taiwan	1999	TCU054	7.62	10.47
31	Chi-Chi, Taiwan	1999	TCU068	7.62	12.17
32	Chi-Chi, Taiwan	1999	TCU075	7.62	5.18
33	Chi-Chi, Taiwan	1999	TCU076	7.62	3.98
34	Chi-Chi, Taiwan	1999	TCU082	7.62	8.98
35	Chi-Chi, Taiwan	1999	TCU087	7.62	9.37
36	Chi-Chi, Taiwan	1999	TCU101	7.62	10.04
37	Chi-Chi, Taiwan	1999	TCU102	7.62	9.74
38	Chi-Chi, Taiwan	1999	TCU103	7.62	8.24
39	Chi-Chi, Taiwan	1999	TCU122	7.62	10.88
40	Chi-Chi, Taiwan	1999	WGK	7.62	4.39

6 References

Abdulridha A, Palermo D, Foo S, Vecchio FJ (2013) Behavior and modeling of superelastic shape memory alloy reinforced concrete beams. Engineering Structures 49:893–904. https://doi.org/10.1016/j.engstruct.2012.12.041

Ahmadi E, Kashani MM (2020) Numerical investigation of nonlinear static and dynamic behaviour of self-centring rocking segmental bridge piers. Soil Dynamics and Earthquake Engineering 128:105876. https://doi.org/10.1016/j.soildyn.2019.105876

Ahmadi E, Kocakaplan S, Kashani MM (2022) Nonlinear seismic fragility analysis of a resilient precast post-tensioned segmental bridge pier. Sustainable and Resilient Infrastructure 7:823–841. https://doi.org/10.1080/23789689.2022.2082644

Applied Technology Council (2009) FEMA P695. Quantification of Building Seismic Performance Factors. 2009. Applied Technology Council

Baker JW (2007) Quantitative classification of near-fault ground motions using wavelet analysis. Bulletin of the Seismological Society of America 97:1486–1501. https://doi.org/10.1785/0120060255

Billington SL, Yoon JK (2004) Cyclic Response of Unbonded Posttensioned Precast Columns with Ductile Fiber-Reinforced Concrete. Journal of Bridge Engineering 9:353–363. https://doi.org/10.1061/(ASCE)1084-0702(2004)9:4(353)

Chou C-C, Chen Y-C (2006) Cyclic tests of post-tensioned precast CFT segmental bridge columns with unbonded strands. Earthquake Engineering & Structural Dynamics 35:159–175. https://doi.org/10.1002/eqe.512

Dawood H, ElGawady M, Hewes J (2012) Behavior of Segmental Precast Posttensioned Bridge Piers under Lateral Loads. Journal of Bridge Engineering 17:735–746. https://doi.org/10.1061/(ASCE)BE.1943-5592.0000252

DesRoches R, Delemont M (2002) Seismic retrofit of simply supported bridges using shape memory alloys. Engineering Structures 24:325–332. https://doi.org/10.1016/S0141-0296(01)00098-0

Hassanli R, Asce SM, Youssf O, Mills JE (2010) Seismic Performance of Precast Posttensioned Segmental FRP-Confined and Unconfined Crumb Rubber Concrete Columns. 1–19. https://doi.org/10.1061/(ASCE)CC.1943-5614.0000789.

Li C, Hao H, Bi K (2017) Numerical study on the seismic performance of precast segmental concrete columns under cyclic loading. Engineering Structures 148:373–386. https://doi.org/10.1016/j.engstruct.2017.06.062

McKenna F (2011) OpenSees: A Framework for Earthquake Engineering Simulation. Computing in Science & Engineering 13:58–66. https://doi.org/10.1109/MCSE.2011.66

Motaref S, Saiidi MS, Sanders DH (1994) Experimental Study of Precast Bridge Columns with Built-In Elastomer. 109–116. https://doi.org/10.3141/2202-14

Ou Y, Asce SM, Chiewanichakorn M, et al (2008) Seismic Performance of Segmental Precast Unbonded Posttensioned Concrete Bridge Columns. 133:1636–1647

Song G, Ma N, Li HN (2006) Applications of shape memory alloys in civil structures. Engineering Structures 28:1266–1274. https://doi.org/10.1016/j.engstruct.2005.12.010

Tazarv M, Saiid Saiidi M (2015) Reinforcing NiTi Superelastic SMA for Concrete Structures. Journal of Structural Engineering 141:1–10. https://doi.org/10.1061/(asce)st.1943-541x.0001176

Wang J, Wang Z (2018) Cyclic loading test of self-centering precast segmental unbonded posttensioned UHPFRC bridge columns. Bulletin of Earthquake Engineering. https://doi.org/10.1007/s10518-018-0331-y

Wang Z, Wang J, Zhu J (2018) Pushover Analysis of Precast Segmental UHPFRC Bridge Columns with Unbonded Posttensioned Tendons. 765:391–396. https://doi.org/10.4028/www.scientific.net/KEM.765.391

Zhang X, Hao H (2019) The response of precast concrete segmental columns subjected to near base impact. https://doi.org/10.1177/2041419618808534